



0191-8141(94)00079-4

Concentrated slip zones with subsidiary shears: their development on three scales in the Cerro Brass fault zone, Appalachian valley and ridge

MARÍA LUISA ARBOLEYA

Departament de Geotectonica, Universitat Autònoma de Barcelona, 08193 Bellaterra (Barcelona), Spain

and

TERRY ENGELDER

Department of Geosciences, The Pennsylvania State University, University Park, PA 16802, U.S.A.

(Received 12 February 1992; accepted in revised form 25 May 1994)

Abstract—Concentrated slip zones bound subsidiary shears at three scales within the Cerro Brass Fault, which cuts Cambrian dolomites of the Nittany Anticlinorium, Pennsylvania. On the outcrop scale thrust faults along both Cerro Brass fault zone boundaries acted as concentrated slip zones bounding subsidiary shears developed along original bedding planes. The outcrop scale subsidiary shears are zones of concentrated slip bounding hand-specimen-scale subsidiary shears. In turn, the hand-specimen-scale subsidiary shears are concentrated slip zones bounding even smaller-scale subsidiary shears. Subsidiary shears in Cerro Brass fault zone are analogous to subsidiary shears (i.e. R_1 and R_2) commonly found in laboratory gouge-friction experiments. The orientations of subsidiary shears at the outcrop and hand-specimen scales define a 'Riedel within Riedel' geometry in which the original bedding played the role of R_1 shears at the outcrop scale and, at the same time, operated as boundary faults at a smaller scale. The presence of subsidiary shears on more than one scale suggests that the Coulomb failure theory is not sufficient to explain their origin.

INTRODUCTION

Some have argued that laboratory experiments are useful analogs for complex natural systems such as fault zones (e.g. Griggs & Handin 1960). The purpose of this paper is to describe a small fault zone in the context of characteristic structures found in experimentally produced fault gouge. Such an exercise is useful in pondering the relevance of laboratory experiments. Starting with early papers on frictional experiments with fault gouge (i.e. Engelder & McKee 1973, Engelder *et al.* 1975), two characteristics of experimentally produced gouge are commonly reported.

First, the most extreme comminution of the gouge occurs at an interface between the gouge and intact rock rather than within the gouge. Extreme comminution at the rock-gouge interface is consistent with an earlier observation that, when quartz powder was sheared between steel, slip took place at the powder-steel interface and not within the powder (Griggs *et al.* 1960). From these observations it is apparent that extreme comminution indicates the location of concentrated slip. Other evidence for concentrated slip at interfaces includes smeared pyrite in calcite gouge (Shimamoto 1977), chatter marks on the rock surface (Logan & Shimamoto 1976), and regions of high shear strain near the interface (Logan *et al.* 1981).

Second, comminution within the gouge layer is most concentrated along distinct, subsidiary shear zones tilted at angles of 10° to 20° to the intact rock-gouge

interface. The acute angle between the subsidiary shear zones and the gouge-rock interface opens towards the direction of slip of the intact rock on the interface. These subsidiary shear zones appear in many experimental gouge types including quartz (Engelder *et al.* 1975, Byerlee *et al.* 1978, Marone & Scholz 1989, Morrow & Byerlee 1989); calcite (Friedman & Higgs 1981); dolomite (Logan & Shimamoto 1976), and even polymineralic natural fault gouge sheared in the laboratory (Logan *et al.* 1981).

Concentrated slip zones bounding subsidiary shears are, indeed, a key element of natural fault zones. A plane of concentrated slip in natural faults is called a principal slip surface or PSS (Sibson 1986). Like finely comminuted laboratory gouge, PSSs are commonly found at one or both margins of a natural fault zone. If found at both margins, the PSSs are also called paired shears (Grocott 1981). The tendency toward concentrated slip favors the development of structural features such as slickenside surfaces (e.g. Power & Tullis 1989) and pseudotachylite (e.g. Grocott 1981). The development of narrow zones of concentrated shear is characteristic of the base of large overthrust sheets including the Glarus thrust, Switzerland (Schmid 1975), the McConnell thrust, Canada (Jamison & Spang 1976), the Muddy Mountain thrust, U.S.A. (Brock & Engelder 1977), and the Esla thrust, Spain (Arboleya 1989). Subsidiary faults are common adjacent to the zone of concentrated shear regardless of the attitude of the fault. For example, evidence points to the generation of subsidiary faults as a

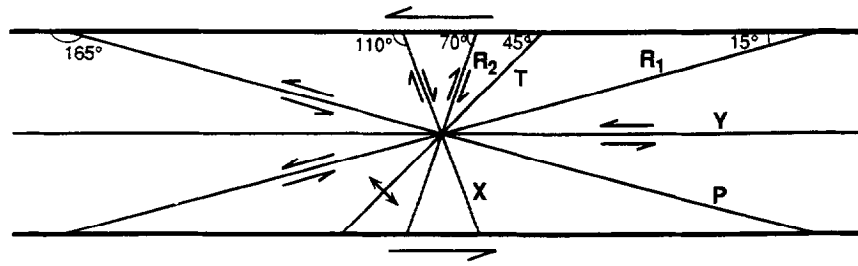


Fig. 1. Cross-sectional view of fracture planes developed in a gouge layer deformed under triaxial conditions (adapted from Logan *et al.* 1979).

critical element in the emplacement of thrust sheets (i.e. Wojtal & Mitra 1986). Strain within the zone of subsidiary shears is necessary to accommodate deformation over irregularities on fault zones. The list of fault zones with subsidiary shears includes the Tizi n'Test Fault Zone, Morocco (Petit 1987), the Fort Foster Brittle Zone, Maine (Swanson 1988), the York Cliffs Fault System, Maine (Swanson 1990), a mining-induced normal fault in South Africa (Gay & Ortlepp 1979), the Motagua fault zone, Guatemala Logan *et al.* (1979), and the Punchbowl fault zone, California (Chester & Logan 1986, 1987).

Terminology

Interest in subsidiary shears was piqued by Riedel (1929) who observed conjugate pairs of subsidiary shear fractures in clay cake experiments. These subsidiary shear fractures are called the Riedel shear, R, and the conjugate Riedel shear, R'. Tchalenko (1970) noted the similarity between Riedel shear fractures in clay cake experiments and subsidiary shear fractures in the soil above the Dasht-e Bayaz earthquake. Geologists were not bashful about applying Riedel's model to large scale faulting associated with the San Andreas fault, again a situation where a fault zone has a free surface (e.g. Chester & Logan 1987). Logan *et al.* (1979) pointed out that subsidiary shear zones within laboratory gouges resemble R and R' shears found in sheared clay cakes. But, because of the difference between boundary conditions in a clay-cake model and the triaxial friction experiment, Logan *et al.* (1979) appropriately adopted a slightly different terminology. R₁ and R₂ refer to subsidiary shear zones in fault gouge produced in natural fault zones formed at depth as well as in triaxial friction experiments whereas R and R' refer to subsidiary shear zones in the surficial expression of strike-slip faults as well as in clay cake models. In addition to the R₁ and R₂ shear sets, Logan *et al.* (1979) noted other planar features in experimental fault gouge including discontinuities found in the T, X, P, and Y orientations (Fig. 1).

THE CERRO BRASS FAULT ZONE

We mapped a thrust fault zone in a cut of Pennsylvania Route 144, in front of the Cerro Brass Company in Bellefonte, Pennsylvania. This fault, which superposes

the Lower member of the Gatesburg Formation (Cambrian) on the Mines Member of the same Formation, is the footwall ramp of a thrust in the core of the Nittany Anticlinorium (Fig. 2a). The structure of the area is characterized by NE-trending fault-bend folds cored by ramp-on-flat thrusts (Fail 1973, Geiser 1988, Srivastava & Engelder 1990).

The Cerro Brass fault zone is bounded by two sub-parallel thrust faults dipping to the southeast (Fig. 3). The internal structure of the fault zone is very complex with rocks so heavily fractured that original bedding is difficult to identify (Fig. 6). Dolomite is most heavily crushed along various subsidiary faults. Little crushing of the rock occurs outside the fault zone. No cleavage is observed inside the fault zone, the footwall or hangingwall. The lower boundary fault dies upward into a bedding-parallel thrust whereas towards the upper part of the outcrop the upper boundary fault continues to cut bedding. Thus, in the upper portion of the outcrop the boundary thrusts are not parallel. Some small faults parallel to the boundary faults occur in the hangingwall, and various sets of joints are also present along the outcrop.

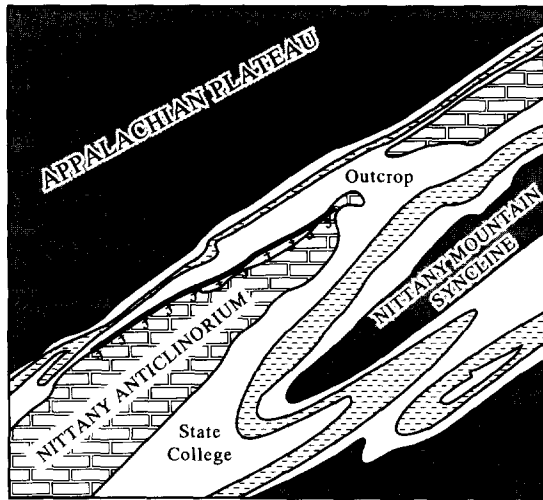
Footwall rocks of the Mines Member are grey dolomites with siliceous oolites and algal laminations with stylolites parallel to bedding. The hangingwall also consists of laminated dolomite and contains a distinct bed of grey sandstone about 1 m thick. This bed is cut by the upper boundary fault in the lower part of the outcrop. The sandstones are made of well-rounded quartz grains with calcareous cement. Locally, quartz overgrowths act as cement. Where the upper boundary fault cuts the sandstone bed, there are scattered quartz grains floating in fault gouge. Cataclastic rocks inside the fault zone are mainly made of dolomite fragments in a matrix of microcrystalline dolomite. Dolomite fragments have calcareous cement and their texture is generally a hypidiomorphic mosaic of subhedral and anhedral dolomite crystals.







STRUCTURES OF THE FAULT ZONE

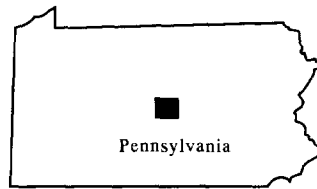
The outcrop scale

The limits of the Cerro Brass fault zone are sharply defined by two boundary faults (BF_O) delimiting a fault zone of about 3.5 m wide. The subscript O refers to outcrop-scale observations (see Table 1 for fault zone

(a)



-  U. Ordovician Clastics and Younger
-  U. Ordovician Carbonates
-  Bellefonte Dolomite
-  M.-L. Ordovician Carbonates
-  Cambrian Carbonates
-  Cerro Brass Thrust



20 km

(b)

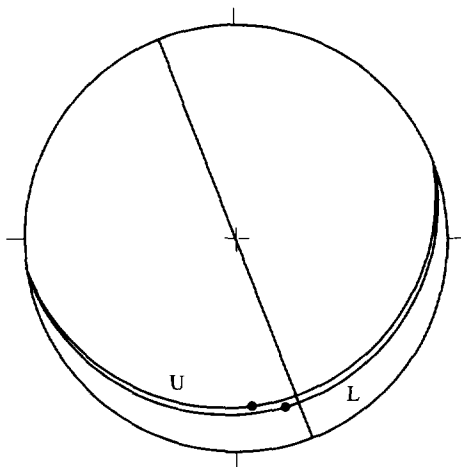


Fig. 2. (a) Location of the Cerro Brass fault zone within the Nittany Anticlinorium. This fault is found on the Geological map of Pennsylvania. (b) Orientation of the boundary faults. U: upper boundary fault, L: lower boundary fault. Dots indicate slip direction from slickensides. Vertical plane on the stereonet shows the strike of the outcrop. Lower hemisphere stereonet projection.

nomenclature). A 5–10 cm thick zone of pale-brown fault gouge of grey dolomite occurs at the contact of the lower BF_O . Parallel to the lower BF_O there are tectonic stylolites, probably related to the induration of the fault

gouge developed on that surface. Fibrous slickensides, found on both BF_O surfaces, show a slip direction towards the north-northwest (Fig. 2b) and indicate that displacement occurred along both bounding surfaces. Thicker and more extensive development of fibrous slickensides on both BF_O suggest greater displacement on these faults than on subsidiary faults. For this reason, each BF_O is a PSS (e.g. Sibson 1986) and is also analogous to the zone of concentrate slip at the rock-gouge contact in fault-gouge experiments (e.g. Engelder *et al.* 1975).

The most prominent feature within the Cerro Brass fault zone is a series of surfaces linking the BF_O but dipping in the opposite direction at a variety of angles (Fig. 6). Slickensides and cataclastic material along some of these subsidiary surfaces show that they are minor faults. The orientation of these subsidiary surfaces with respect to the boundaries of the fault zone is similar to subsidiary shears found in both natural fault zones such as the Dasht-e Bayaz fault (Tchalenko 1968, Tchalenko & Ambraseys 1970) and fault-gouge experiments (Logan *et al.* 1979). We label these subsidiary faults R_{1-O} (see Table 1). The subscript 1 refers to subsidiary shears formed at depth (vs those found in soil) and the subscript O refers to an outcrop scale observation. The angle between the R_{1-O} and BF_O of the Cerro Brass fault zone varies about an average of 26° . The orientation of shears was measured counterclockwise from the boundary faults defining the fault zone. Considering that the fault zone cuts bedding at 15° , the R_{1-O} may have started as bedding surfaces which were rotated about 10° as passive markers inside the fault zone.

Inside zones bounded by R_{1-O} , a set of more steeply dipping fractures makes an angle of about 70° to BF_O . This orientation coincides with that of conjugate R_{2-O} (Logan *et al.* 1979). There are no fractures dipping in the same sense as the boundary faults (P fractures) nor are there any features that could be identified as tensile cracks (T fractures) at this scale inside the fault zone. Beneath the upper boundary fault and parallel to it, on the lowest part of the outcrop, there are some small fractures of decimetric scale which may be similar to Y fractures.

The hand-specimen scale

In order to study structures at the hand-specimen scale, oriented samples were cut perpendicular to the main fault surface (BF_O) and parallel to the slip direction on the boundary faults viewed looking to the northeast in the same perspective as the outcrop photographs. In some of the samples the rock in contact with either R_{1-O} or BF_O is a breccia with fragments no larger than 2 cm, but at a small distance from the contact the rock texture is defined by numerous small faults, some with an obvious sense of shear. When observed at hand-specimen scale, the fault zone shows a complicated fracture pattern that resembles the geometry found at the outcrop scale. This type of geometry was called

'Riedel within Riedel' by Tchalenko (1970). In the Cerro Brass fault zone, the R_{1-O} , subsidiary faults at the outcrop scale, appear to play the role of boundary shears at the hand-specimen scale so that they are also labeled BF_H where the subscript H refers to observations on the hand-sample scale (Table 1).

At hand-sample scale, fractures have a wide range of orientations, and it is difficult to separate them into sets (Figs. 7a–c and 8a). A shear fracture set subsidiary to BF_H is well developed in all the hand samples. This small-scale subsidiary set is labeled R_{1-H} . The R_{1-H} form at angles less than 20° to the BF_H (i.e. R_{1-O}). Occasionally along the R_{1-H} , the original rock was comminuted into 2 mm thick zones of white gouge from which no sense of shear can be deduced. Between the R_{1-H} another set of prominent fractures forms at angles of $\sim 70^\circ$ to BF_H and shows a shear character that is conjugate to R_{1-H} . These conjugates are similar to the R_2 shear set observed by Logan *et al.* (1979) and, hence, are labeled R_{2-H} .

Fractures inclined at 45° to BF_H have no obvious sense of displacement and, hence, are labeled T_H fractures. Fractures making angles larger than 100° within the fault are rare, although there are some making an angle of about 160° with a sense of shear consistent with that of P_H shears. In some samples narrow zones of intense comminution are parallel to the boundary faults (Fig. 4). Their disposition is equivalent to Y_H planes.

The microscopic scale

Deformation at the microscopic scale is mainly cataclastic with minor ductile behavior as indicated by f ($0\bar{2}\bar{2}1$) twinning in dolomite crystals. The number of twinned grains does not exceed one in three. The fracture pattern observed at this scale is consistent with that found at the hand-specimen scale. Because of intense cataclasis, only some fault rocks still preserve the original texture of microscopic subsidiary shears (R_{1-M}). As cataclasis increases, the subsidiary fracture pattern becomes more complex and the identification of individual shears becomes problematic. The most pronounced features at the microscopic scale are narrow zones of intense deformation either at the bounding fault surfaces or parallel to them (Y_M surfaces) composed of dolomite fault gouge. Such zones have a sharp contact with the surrounding rock. Gouge is often injected from these zones into subsidiary fractures as seen in Figs. 5(a) & (b).

The BF_M , which are the R_{1-H} , show a significant degree of grain size reduction but generally it is not possible to determine a shear sense from them. R_{1-M} consists of a matrix of brown color containing dolomite fragments of variable size. R_{2-M} shears produce a variable degree of comminution and their clockwise sense of slip, which can be established in some cases (Fig. 4a), is consistent with slip on adjacent BF_M .

The existence of T_M fractures is also problematic. In some samples, extension fractures with irregular but mated walls are filled with indurate gouge injected

between them (Figs. 5a & b). Nevertheless in other cases fractures at 45° of the fault surface show evidence of shear displacement (Fig. 4b). This is interpreted as a consequence of later shear on previously formed T_M fractures. In the case of Y_M shears, the extensive grain size reduction indicates a large shear displacement along these surfaces (Fig. 4b).

Rotation of fabric elements

Subsidiary faults form during distributed shear strain within the fault zone. Once formed, subsidiary faults rotate as passive markers during further shear strain. Rotation takes place with the same sense of shear as the overall fault zone when viewed looking to the northeast (Fig. 9). This is particularly apparent at the hand-specimen scale. Because the Cerro Brass fault zone had a sinistral sense of displacement, outcrop-scale subsidiary faults were subjected to a counterclockwise rotation. The amount of rotation depends on the amount of displacement on the boundary faults and on the initial orientation of each subsidiary fracture within the shear zone (Ramsay & Huber 1983). Rotation of subsidiary shears may lead to the superposition of two different sets of fractures (see Fig. 9).

Sample A-8 (Figs. 7a & b) contains a boundary fault surface, BF_H . In the contact with the fault surface there is a tectonic breccia with dolomite fragments smaller than 2 cm contained in a cataclastic matrix including calcite grains. The subsidiary faults at angles of about 14° to the BF_H are identified as R_{1-H} . Along these subsidiary faults is a 2 mm thick white gouge from which no sense of displacement can be deduced. Between two consecutive R_{1-H} there is another set of faults making angles of about 60° to the R_{1-H} and showing a clockwise sense of shear compatible with that deduced for the main fault. At this scale these are the R_2 of Logan *et al.* (1979). Assuming that our interpretation of R_{1-H} is correct, these shear zones should display a counterclockwise sense of shear when facing the outcrop and looking northeast.

Zone A in sample A-8 shows a higher degree of comminution than the rest of the zones; the long axes of the fragments inside it are not R_{2-H} shears (Fig. 4a). Fractures in this zone are oriented at very high angles to the boundary fault (BF_H) as is expected for P shears. The boundaries of zone A (R_{1-H}) are displaced by the R_{2-M} shears developed outside that zone (Figs. 4a and 7c) indicating that R_{2-M} shears followed the development of zone A. This conclusion is also supported by the injection of fine gouge from zone A into R_{2-M} shears below that zone (Fig. 4a).

Another portion of sample A-8 (Fig. 7b) also contains fractures making high angles with the fault surface, some of them showing evidence of internal clockwise shearing consistent with R_{2-H} shears. The orientation of these shears at angles higher than 70° to BF_H is consistent with sinistral slip on the BF_H . Note that while internal shear of R_{2-H} is clockwise, the external rotation of the zone relative to BF_O is still counterclockwise. Fractures in the

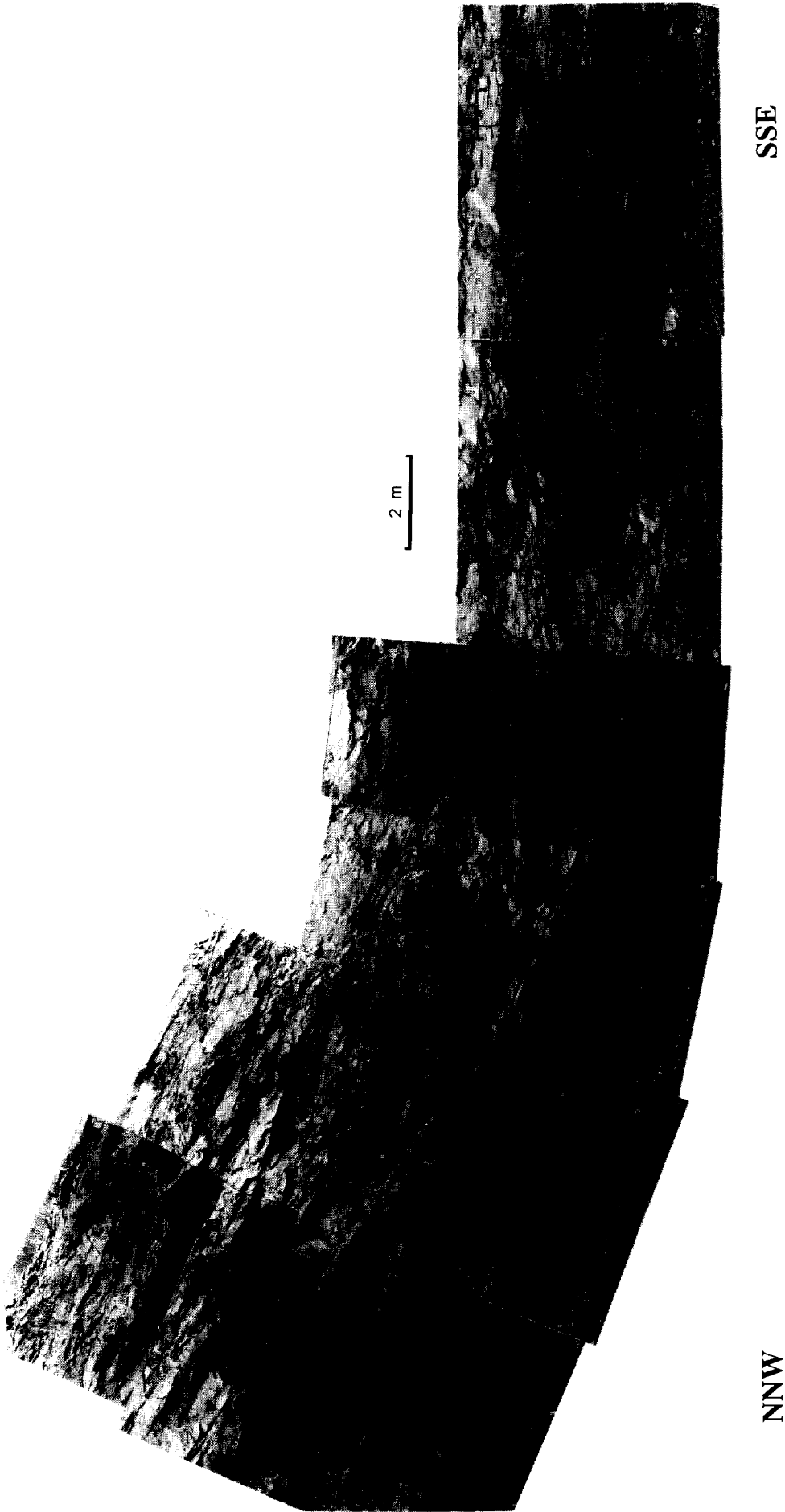


Fig. 3. Photo-mosaic of the Cerro Brass fault zone looking toward the northeast. In the lower part of the outcrop the fault zone width is 3.7 m. Distortion of the outcrop due to its slightly curved shape exaggerates real dips. This study is based on observations taken in the lowest portion (3 m high) of the outcrop.

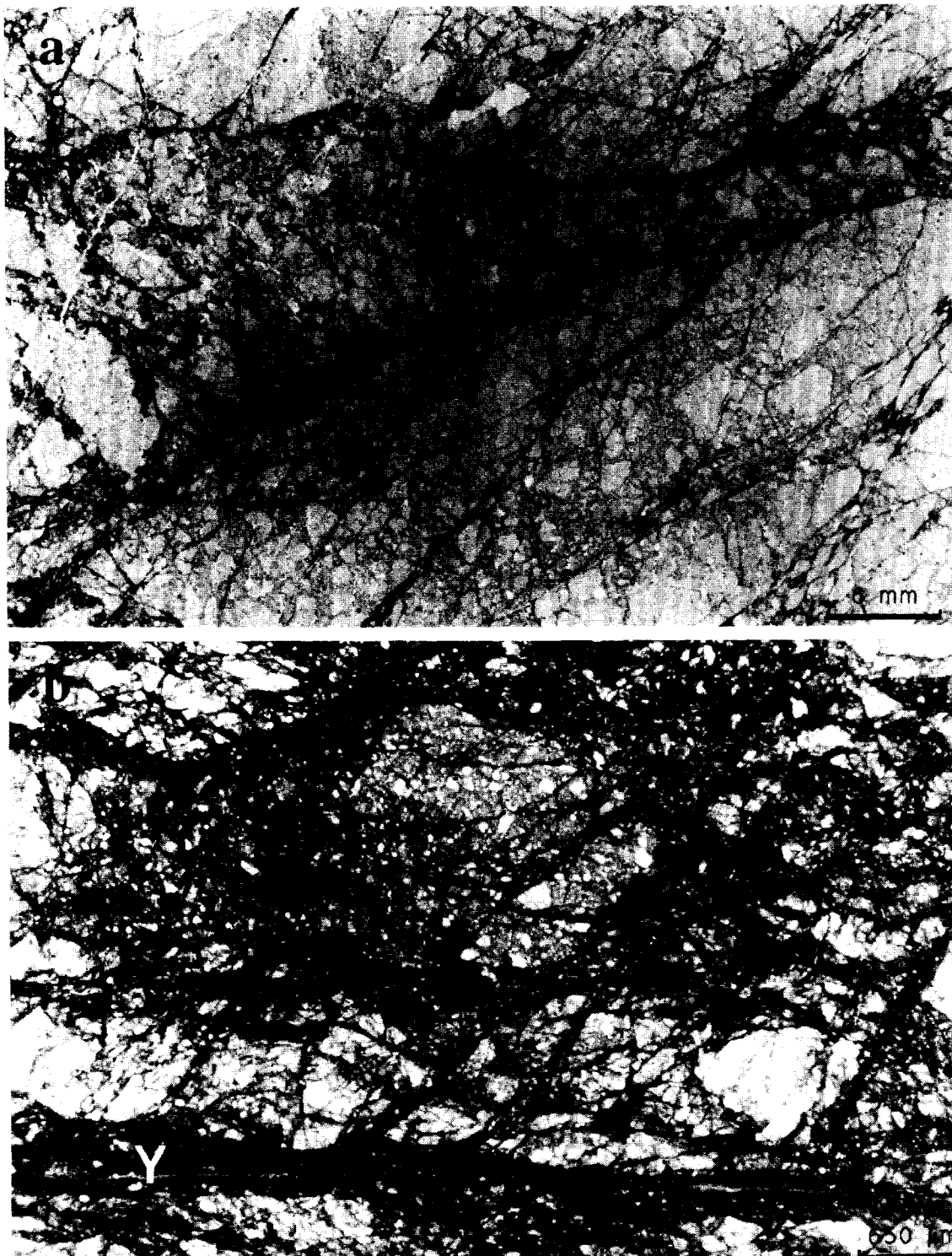


Fig. 4. (a) Photomicrograph of sample A-8 (Fig. 7c) showing shear displacement on R_2 at the upper border of zone A (Fig. 7a) and gouge injection in these shears below zone A. (b) Photomicrograph of sample A-15 showing Y-shear with important comminution (Y), and fractures at 45° to it, with shear displacement and filled with gouge.

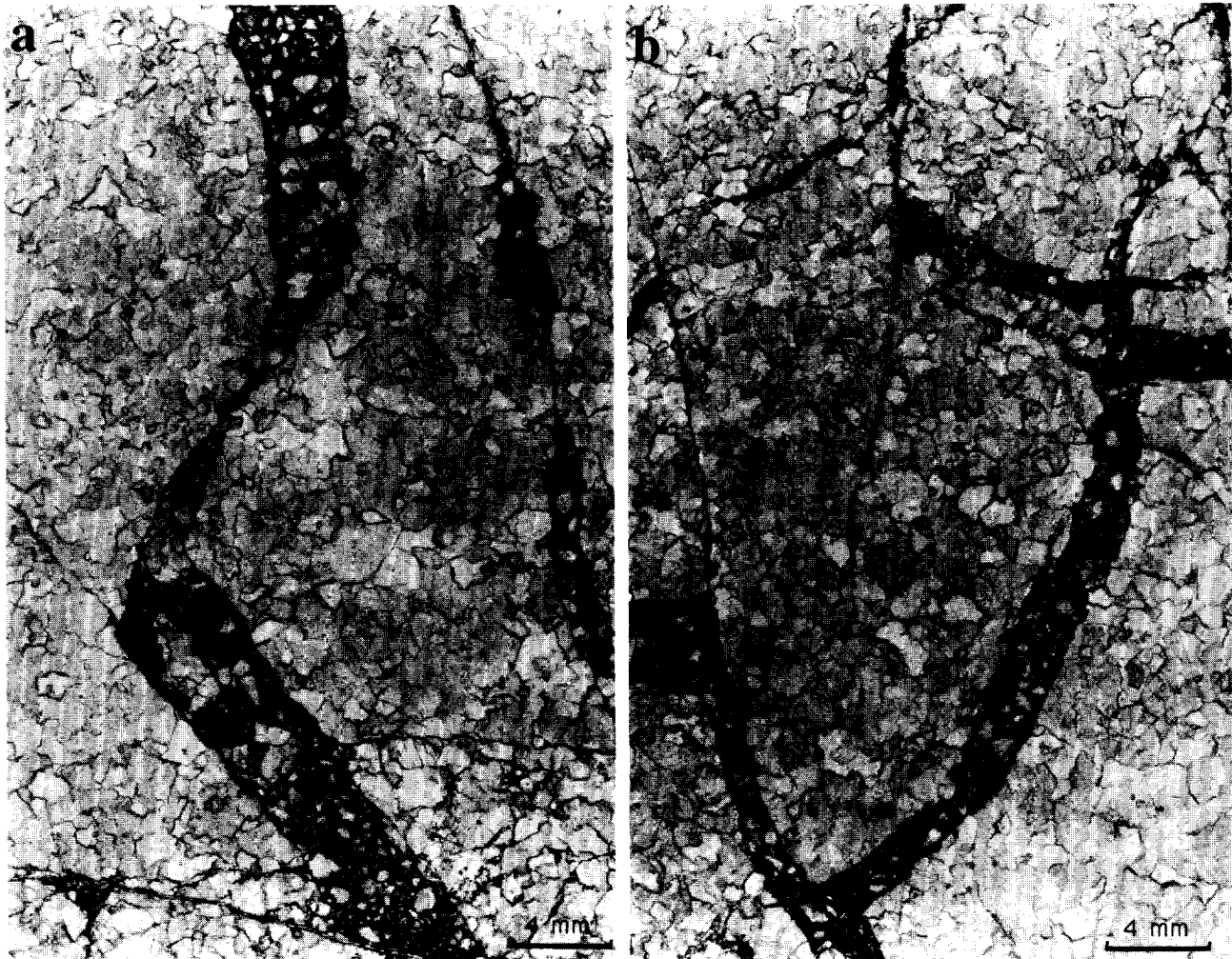


Fig. 5. Photomicrograph of sample A-8 showing opening fractures filled with injected gouge. Note that the walls can be joined together suggesting that a crack propagation mechanism was active during comminution.

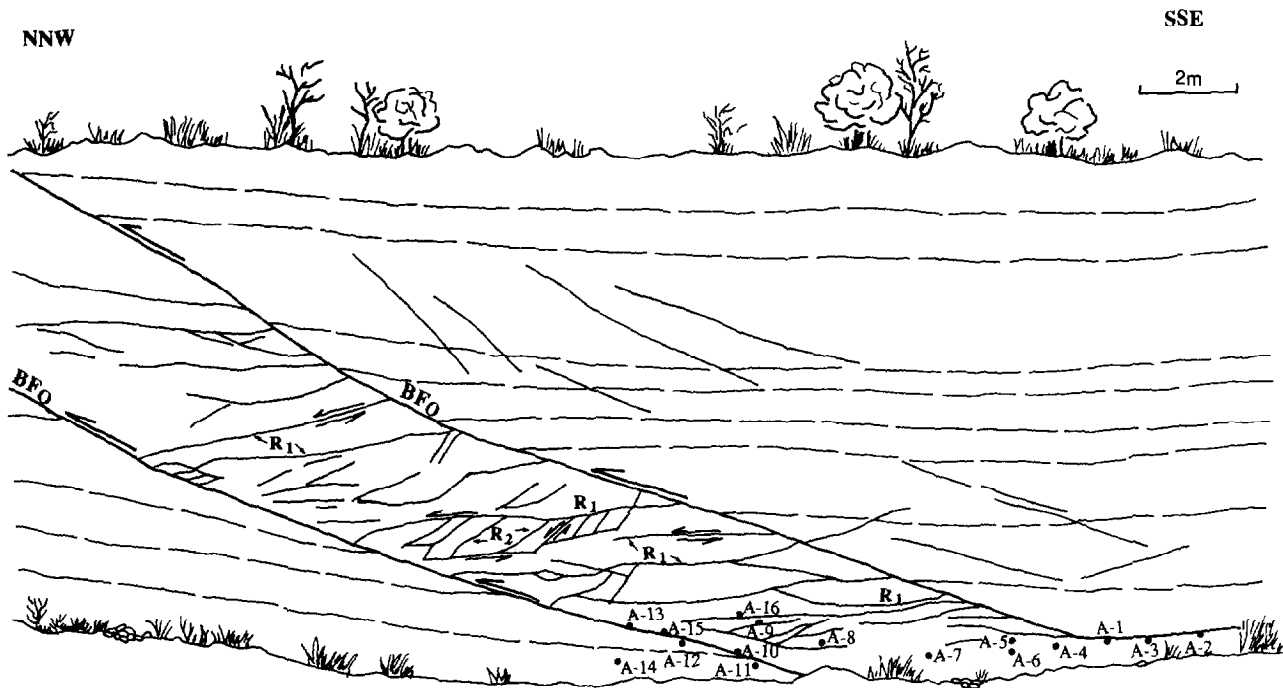


Fig. 6. Sketch of the fault zone showing the boundary thrust folds (BF_O), the internal structures including R₁ (R_{1-O} = BF_H) and R₂ (R_{2-O}) fractures. Numbers give sample locations.

Table 1. Fault-zone nomenclature at the scales considered. BF = Boundary Fault, O = Outcrop scale, H = Hand specimen scale and M = Microscopic scale

Scale	Boundary fault	Subsidiary shear
Outcrop	Cerro Brass thrusts BF _O	R _{1-O}
Hand specimen	R _{1-O} becomes BF _H	R _{1-H}
Microscopic	R _{1-H} becomes BF _M	R _{1-M}

X_H set orientation are less frequent although are present in some of the samples. Apart from zone A in sample A-8, only one of our hand specimens (A-10) contains an appreciable number of P_H shears oriented at very high angles (166°) to the shear direction.

The orientation histogram for sample A-8 at hand specimen scale (Fig. 8c) shows a composite high peak of R_{2-H} shear fractures showing effects of counterclockwise rotation from initiation angle (70°) to higher angles, and another angle peak between 10° and 20° representing R_{1-H}. The peak between 40° and 100° corresponds to T_H and R_{2-H} sets forming at 45° and 70°, respectively, and then rotating counterclockwise. The small peak at 100°–120° is due to the poor development of the X_H set. Fractures inside zone A give a maximum at approximately 160° showing the presence of P_H shears.

Sample A-12 shows a fracture pattern at hand specimen scale (Fig. 8a) in which R_{1-H} and T_H fractures are the best developed. An orientation histogram showing the subsidiary fractures for this sample (Fig. 8b) has a composite peak dominated by R_{1-H} and T_H sets. The relative maximum between 8° and 16° corresponds to the initial orientation of R_{1-H}. A counterclockwise rotation of the set towards higher angles is evident. Tension fractures (T_H) are represented by a relative maximum at approximately 45°, their subsequent rotation towards

higher angles gives another peak between 56° and 64°. The small peak at 70°–80° reveals the existence of less common R_{2-H} faults.

The orientation histogram for fractures at microscopic scale in sample A-8 (Fig. 8d) presents a peak at 60°–70° corresponding to the orientation of R_{2-M} shears and shows effects of counterclockwise rotation to higher angles (80°–90°) due to shearing. T_M fractures also show a certain degree of rotation. The small peak at approximately 120° is due to the presence of X_M shears and the higher one at 160° corresponds to P_M shears developed in zone A.

Sample A-10 at microscopic scale (Fig. 8e) shows a more complete pattern of subsidiary faults. The higher peak corresponds to a maximum at about 160° attributed to P shears probably rotated counterclockwise to higher angles and to the presence of Y shears oriented at 170°–180° of the BF_M. The R_{1-M} are well represented by a peak at less than 20° and show evidence of rotation towards higher angles. Fractures of the T_M orientation are poorly developed. The R_{2-M} set show a broad distribution between 60° and 110° with a maximum at approximately 70° (their initial orientation) and another maximum at 90° probably due to rotation. A smaller peak around 120° corresponds to X_M shears.

DISCUSSION

The concept of self-similar fault zones

If an object is self-similar its shape is the same regardless of the scale on which it is viewed. Self-similarity is often measured by a shape factor called a fractal dimension. The particle size-distribution during the formation

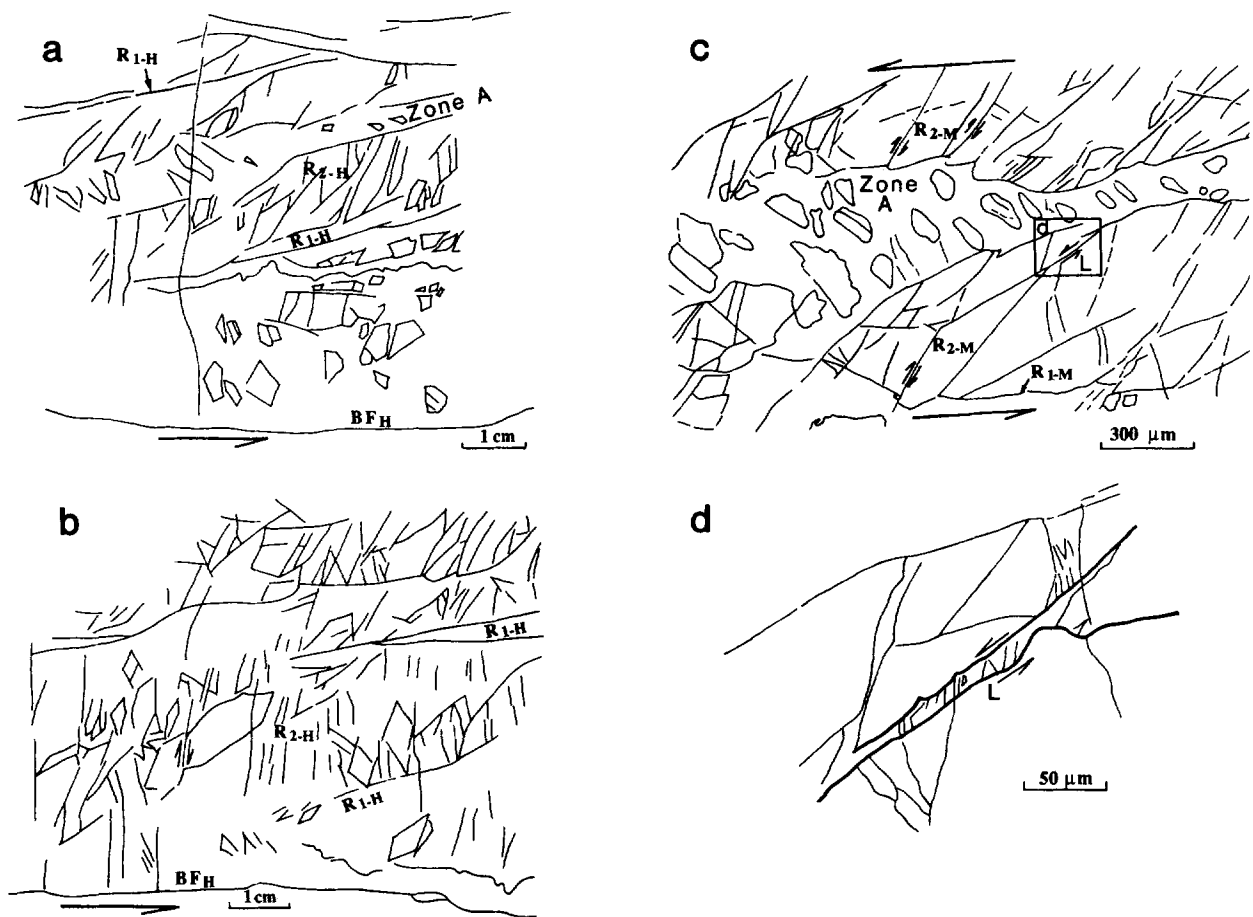


Fig. 7. Sketches of sample A-8. (a) Sketch of the hand specimen showing R_{1-H} and R_{2-H} shears and the position of zone A. (b) Another section of the hand specimen showing mainly R_{2-H} faults with a few R_{1-H} . (c) Microscopic sketch showing the internal structure of zone A and the relative sense of slip on R_{2-M} . (d) Enlargement of framed area in (c) showing the structure inside fracture L.

of fault gouge is fractal (Sammis *et al.* 1987) and can be generated by failure at loading-bearing bridges (Biegel *et al.* 1989). On a much larger scale the geometry of fault traces is also self-similar (Aviles *et al.* 1987, Okubo & Aki 1989). Finally, the b -value behavior of earthquake faults is a consequence of three-dimensional self-similar fault geometry (King 1983).

In our description of the Cerro Brass fault zone, we have suggested that boundary faults and subsidiary shears appear the same on three scales: the outcrop, the hand specimen; and the thin section (Fig. 10). This pattern of subsidiary shears suggests that the Cerro Brass fault zone approximates a self-similar body. One implication of self-similar subsidiary shears is that they may reflect the local reorientation of the stress field, a phenomenon recently observed in the vicinity of the San Andreas fault (Mount & Suppe 1987) and the San Gabriel fault zone (Chester 1991, personal communication). With application to the Cerro Brass fault zone, this interpretation presents a problem as described below.

The local stress field and 'Riedel within Riedel' structures

The Cerro Brass fault zone contains an internal structure of the type 'Riedel within Riedel' as described by

Tchalenko (1970). This geometry poses an interesting problem concerning stress field orientation relative to the development of subsidiary shear fractures at different scales. In the analysis of Riedel shears, there is general agreement that border faults are planes of maximum shear stress and, hence, the local σ_1 is oriented at 45° to the border faults for both clay-cake models and triaxial gouge-friction experiments (i.e. Tchalenko & Ambraseys 1970, Tchalenko 1970, Mandl *et al.* 1977, Logan *et al.* 1979). Furthermore, analyses assume that Riedel shears develop in rock or gouge exhibiting Coulomb behavior so that the shears are interpreted in terms of the Coulomb failure criterion. If so, the angle, α , between the border faults and subsidiary shears, R_1 is $\phi/2$ where ϕ is the coefficient of internal friction for a Coulomb material ($\alpha = \phi/2$).

At the hand-sample and microscopic scale we measure an angle for α of about 15° . Interestingly, this is the same value measured by Logan *et al.* (1979) for subsidiary shears in fault gouge. On the outcrop scale the angle, α , is somewhat larger but we expect this may arise by a combination of effects including capture of bedding planes as subsidiary shears and subsequent counterclockwise rotation of these planes. The Cerro Brass fault zone develops subsidiary faults on three scales and by analogy with laboratory experiments the

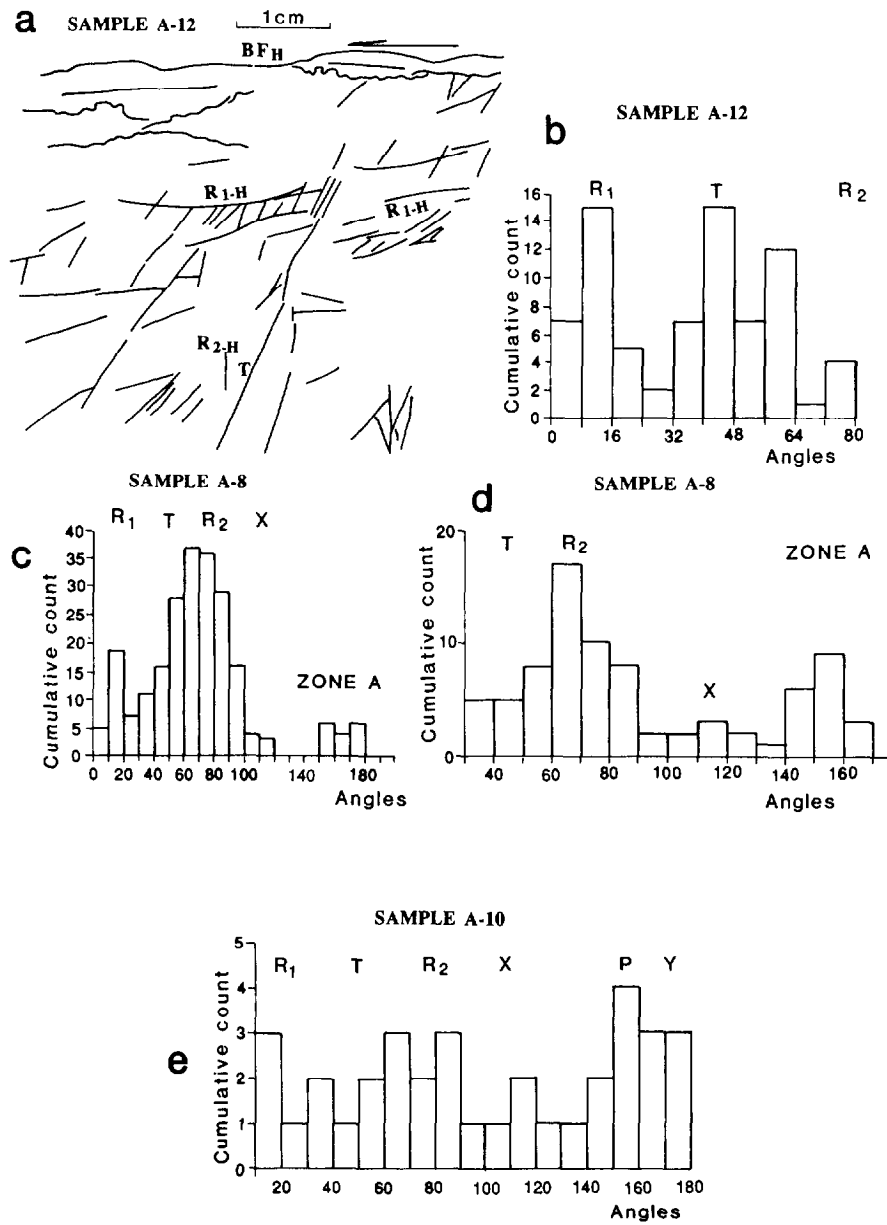


Fig. 8. (a) Sketch of the fracture array at hand-specimen scale in sample A-12 situated below the lower thrust (BF_O). (b) Histogram showing the angles between the thrust (BF_O) surface and shear and tension fractures in sample A-12 at hand-specimen scale. (c) Histogram showing the angles between the boundary fault (BF_H) and the shear and tension fractures in sample A-8 at hand-specimen scale. (d) Histogram showing the angles between the boundary faults and shear fractures in samples A-8 at microscopic scale. (e) Histogram showing the angles between the boundary faults and shear fractures in sample A-10 at microscopic scale.

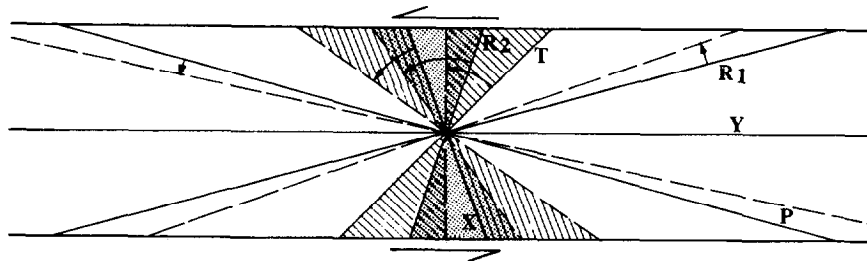


Fig. 9. Rotation of subsidiary fractures inside a sinistral fault zone as consequence of slip on the fault zone borders. Full lines represent the original orientation of fractures after Logan *et al.* (1979). Discontinuous lines show the orientation of fractures after a shear strain $\gamma = 1$. Note that rotation of T superimposes that fracture set on R₂, and rotation of R₂ makes it to superpose on X fractures. Note also that the amount of rotation is different for each original orientation.

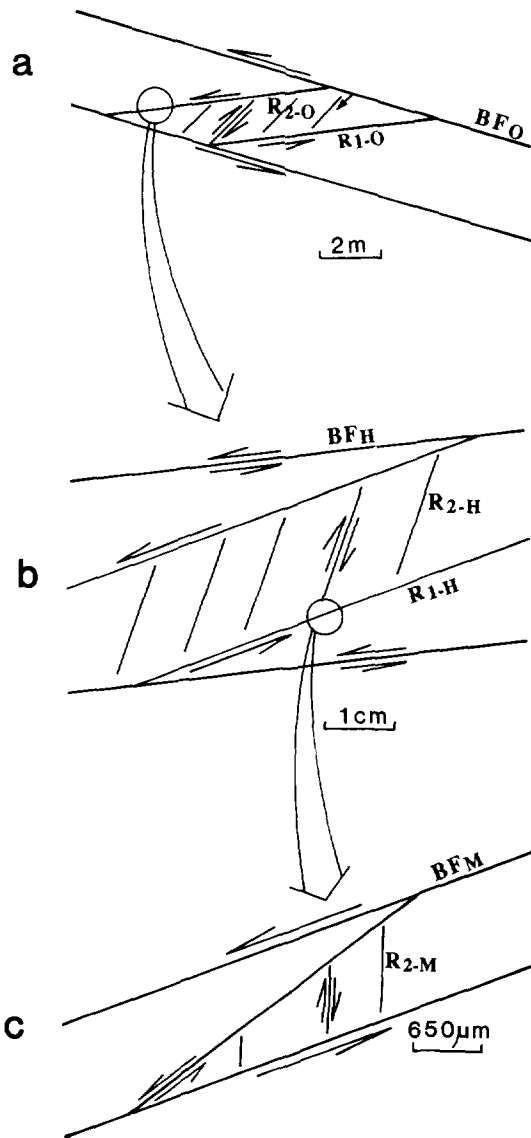


Fig. 10. Relative orientation of fractures at the scales considered. (a) Outcrop scale. (b) Hand-specimen scale. (c) Microscopic scale.

behavior at each scale consistent with a Coulomb material.

In the geologic setting of thrust faults such as the Cerro Brass, the regional stress field is defined by a horizontal σ_1 and a vertical σ_3 (Anderson 1951). Presumably, the fault zone develops by Coulomb failure with a small dip (15°) relative to a horizontal σ_1 . Once the boundary faults (BF_O) develop, the local stress field must reorient in the vicinity of the fault. With the BF_O dipping at 15° the orientation of the local σ_1 responsible for the generation of the subsidiary shears should be $45^\circ - \phi/2 - 15^\circ = 30^\circ - \phi/2$ to the horizontal; that is, the local σ_1 plunges 30° toward the BF_O . T fractures would also be related to this orientation of σ_1 as they grow parallel to the maximum compressive stress (Hancock 1972, Vialon 1979). This is a local stress field on the outcrop scale.

As the Cerro Brass fault zone is a 'Riedel within Riedel' structure the R_{1-O} also act as boundary shear zones inside which other R_{1-H} and R_{2-H} develop and, in turn, R_{1-H} act to bound subsidiary shears R_{1-M} . If the R

fractures at smaller scales are Coulomb fractures, then local σ_1 at these smaller scales would rotate even further in the same sense as the shear movement and become steeper. From this exercise arises the dilemma that the apparent orientation of σ_1 depends on the scale on which the fault is viewed. Tchalenko (1970), Gamond (1983) and Mandl (1988) observed a rotation of local maximum stresses in the region of overlapping of Riedel shears that causes the development of P shears. In such conditions the R_{1-H} will not act as a maximum shear stress planes and will not be in the orientation to develop Riedel shears at a smaller scale. Yet, we observe them. In this case, the generation of subsidiary shears at different scales cannot be explained in terms of a scale-independent Coulomb theory. For this reason, the notion of self-similarity seems inappropriate when viewing subsidiary shears.

The applicability of the Coulomb theory to Riedel shears is under discussion. Moore *et al.* (1989) and Moore & Byerlee (1991) showed that Coulomb theory does not explain the observed Riedel angles and found these angles correlated with the sliding behavior, showing that changes in the parameters controlling sliding behavior affect the orientation of subsidiary shears. Moore & Byerlee (1992) and Byerlee (1992) found that the orientation and relative proportion of R and P shears is controlled by fluid pressure.

The mechanism for formation of subsidiary shears still remains unclear. For example, some fractures and faults with very little shear displacement exhibit pinnate joints which cut the planar surface at a small angle ($<20^\circ$) (Engelder 1989). As such, pinnate joints fall in the same orientation as R_1 shears, and so it is easy to mistake one for the other. Furthermore, microcracks within larger quartz-gouge particles often propagate at very small angles to the subsidiary planes (Engelder 1974). In fact, Petit (1987) suggests that some R_1 shears are pinnate joints reactivated in shear. Swanson (1988, 1990) interprets some of the fracture sets (R , R' , T_1 , P^*) as due to layer parallel simple shear, others (X , X' , T_2) as related to layer-parallel extension, and others (P , P' , T_3) as related to layer-parallel shortening. We are now left to wonder how the same stress field operates on different scales to produce similar structures with different orientation relative to the remote principal stresses.

CONCLUSIONS

The Cerro Brass fault zone has undergone a heterogeneous deformation. Displacement inside it has taken place along localized shear planes of various types at different scales: boundary (thrust) faults; original bedding planes (R_{1-O}); shear fractures (R_{1-H} and R_{1-M}) and X and Y shears after Tchalenko (1968) and Logan *et al.* (1979). The relative orientation of the shear planes at the outcrop and at the hand-sample scales defines a 'Riedel within Riedel' geometry (Tchalenko 1970) in which the original bedding played the role of R_{1-O} shears

and, at the same time, operates as boundary faults, BF_H, at a smaller scale. Boundary faults with subsidiary shears are also found at the microscopic scale. This type of behavior is not consistent with a scale-dependent Coulomb fracture criterion.

Acknowledgements—This work was carried out while M. L. Arboleya was visiting professor at the Geosciences Department of the Pennsylvania State University. The work financed by the Ministerio de Educacion y Ciencia (D.G.I.C.Y.T.) of Spain (M.L.A.), EPRI contract RP 2556-24 (T.E.) and a grant from Texaco (T.E.). Thanks are given to I. Zamarréno for her help on dolomite textures. We thank Mark Swanson and Steve Wojtal for comments on an earlier version of this paper.

REFERENCES

- Anderson, E. M. 1951. *The Dynamics of Faulting and Dyke Formation with Application to Britain*, 2nd edn. Oliver and Boyd, London.
- Arboleya, M. L. 1989. Fault rocks of the Esla thrust (Cantabrian Mountains, N. Spain): An example of foliated cataclasites. *Annales Tect.* **3**, 99–109.
- Aviles, C. A., Scholz, C. H. & Boatwright, J. 1987. Fractal analysis applied to characteristic segments of the San Andreas fault. *J. geophys. Res.* **92**, 331–344.
- Biegel, R. L., Sammis, C. G. & Dieterich, J. H. 1989. The frictional properties of a simulated gouge with a fractal particle distribution. *J. Struct. Geol.* **11**, 827–846.
- Brock, W. G. & Engelder, T. 1977. Deformation associated with the movement of the Muddy Mountain overthrust in the Buffington window, southeastern Nevada. *Bull. geol. Soc. Am.* **88**, 1413–1420.
- Byerlee, J. 1992. The change in orientation of subsidiary shears near faults containing pore fluid under high pressure. *Tectonophysics* **211**, 295–303.
- Byerlee, J., Mjachkin, V., Summers, R. & Voevoda, O. 1978. Structures developed in fault gouge during stable sliding and stick-slip. *Tectonophysics* **44**, 161–171.
- Chester, F. M. & Logan, J. M. 1986. Implications for mechanical properties of brittle faults from observations of the Punchbowl fault zone, California. *Pure & Appl. Geophys.* **124**, 79–106.
- Chester, F. M. & Logan, J. M. 1987. Composite planar fabric gouge from the Punchbowl Fault, California. *J. Struct. Geol.* **9**, 621–634.
- Engelder, T. 1974. Cataclasis and the generation of fault gouge. *Bull. geol. Soc. Am.* **85**, 1515–1522.
- Engelder, T. 1989. The analysis of pinnate joints in the Mount Desert Island Granite: Implications for post-intrusion kinematics in the coastal volcanic belt, Maine. *Geology* **17**, 564–567.
- Engelder, T. & McKee, T. R. 1973. Electron microscopical study of indurated quartz gouge. *Proc. 31st Ann. Electron Microscopy Soc. Am.* 214–215.
- Engelder, T., Logan, J. M. & Handin, J. 1975. The sliding characteristics of sandstone on quartz fault-gouge. *Pure & Appl. Geophys.* **113**, 69–86.
- Faill, R. T. 1973. Kink band folding, Valley and Ridge Province, Pennsylvania. *Bull. geol. Soc. Am.* **84**, 1289–1314.
- Friedman, M. & Higgs, N. G. 1981. Calcite fabrics in experimental shear zones. In: *Mechanical Behavior of Crustal Rocks* (edited by Carter, N. L., Friedman, M., Logan, J. M. & Stearns, D. W.). *Am. Geophys. Un. Geophys. Monogr.* **24**, 11–27.
- Gamond, J. F. 1983. Displacement features associated with fault zones: a comparison between observed examples and experimental models. *J. Struct. Geol.* **5**, 33–45.
- Gay, N. C. & Ortlepp, W. D. 1979. Anatomy of a mining-induced fault zone. *Bull. geol. Soc. Am.* **90**, 47–58.
- Geiser, P. A. 1988. The role of kinematics in the construction and analysis of geological cross-sections in deformed terranes. In: *Geometries and Mechanisms of Thrusting* (edited by Mitra, G. & Wojtal, S.). *Spec. Pap. geol. Soc. Am.* **222**, 47–76.
- Griggs, D. T. & Handin, J. (Eds) 1960. Rock deformation. *Mem. geol. Soc. Am.* **79**, 1–352.
- Griggs, D. T., Turner, F. J. & Heard, H. C. 1960. Deformation of rocks at 500°C to 800°C. In: *Rock Deformation* (edited by Griggs, D. T. & Handin, J.). *Mem. geol. Soc. Am.* **79**, 39–104.
- Grocott, J. 1981. Fracture geometry of pseudotachylite generation zones: a study of shear fractures formed during seismic events. *J. Struct. Geol.* **3**, 169–179.
- Hancock, P. L. 1972. The analysis of en-échelon veins. *Geol. Mag.* **109**, 176–269.
- Jamison, W. R. & Spang, J. H. 1976. Use of calcite to infer differential stress. *Bull. geol. Soc. Am.* **87**, 868–872.
- King, G. 1983. The accommodation of large strains in the upper lithosphere of the earth and other solids by self-similar fault systems: the geometrical origin of *b*-value. *Pure & Appl. Geophys.* **121**, 761–815.
- Logan, J. M. & Shimamoto, T. 1976. The influence of calcite gouge on frictional sliding of Tennessee sandstone. *EOS* **57**, 1011.
- Logan, J. M., Friedman, M., Higgs, N., Dengo, C. & Shimamoto, T. 1979. Experimental studies of simulated gouge and their application to studies of natural fault zones. In: *Analysis of Actual Fault Zones in Bedrock. U.S. geol. Surv. Open-file Rept.* **79-1239**, 305–343.
- Logan, J. M., Higgs, N. G. & Friedman, M. 1981. Laboratory studies on natural gouge from the U.S. Geological Survey Dry Lake Valley No. 1 well, San Andreas fault, California. In: *Mechanical Behavior of Crustal Rocks* (edited by Carter, N. L., Friedman, M., Logan, J. M. & Stearns, D. W.). *Am. Geophys. Un. Geophys. Monogr.* **24**, 121–134.
- Mandl, G. 1988. *Mechanics of Tectonic Faulting*. Elsevier, New York.
- Mandl, G., de Jong, L. N. J. & Maltha, A. 1977. Shear zones in granular material. An experimental study of their structure and mechanical genesis. *Rock Mechanics* **9**, 95–144.
- Marone, C. & Scholz, C. H. 1989. Particle-size distribution and microstructures within simulated fault gouge. *J. Struct. Geol.* **11**, 799–814.
- Moore, D. E. & Byerlee, J. D. 1991. Comparative geometry of the San Andreas fault, California, and laboratory fault zones. *Bull. geol. Soc. Am.* **103**, 762–774.
- Moore, D. E. & Byerlee, J. D. 1992. Relationships between sliding behavior and internal geometry of laboratory fault zones and some creeping and locked strike-slip faults of California. *Tectonophysics* **211**, 305–316.
- Moore, D. E., Summers, R. & Byerlee, J. D. 1989. Sliding behavior and deformation textures of heated illite gouge. *J. Struct. Geol.* **11**, 329–342.
- Morrow, C. A. & Byerlee, J. D. 1989. Experimental studies of compaction and dilatancy during frictional sliding on faults containing gouge. *J. Struct. Geol.* **11**, 815–825.
- Mount, V. & Suppe, J. 1987. State of stress near the San Andreas fault. Implications for wrench tectonics. *Geology* **15**, 1143–1146.
- Okubo, P. G. & Aki, K. 1989. Fractal geometry in the San Andreas fault system. *J. geophys. Res.* **92**, 345–356.
- Petit, J.-P. 1987. Criteria for sense of movement on fault surfaces in brittle rocks. *J. Struct. Geol.* **9**, 597–608.
- Power, W. L. & Tullis, T. E. 1989. The relationship between slicken-sid surfaces in fine-grained quartz and the seismic cycle. *J. Struct. Geol.* **11**, 879–894.
- Ramsay, J. G. & Huber, M. I. 1983. *The Techniques of Modern Structural Geology, volume I: Strain Analysis*. Academic Press, London.
- Riedel, W. 1929. Zur Mechanik geologischer Brucherscheinungen. *Zentralbl. Min. Geol. und Pal.* **1929 B**, 354–368.
- Sammis, Ch., King, G. & Biegel, R. 1987. The kinematics of gouge deformation. *Pure & Appl. Geophys.* **125**, 777–812.
- Schmid, S. M. 1975. The Glarus overthrust: Field evidence and mechanical model. *Ecol. geol. Helv.* **68**, 247–280.
- Shimamoto, T. 1977. Effects of fault-gouge on the frictional properties of rocks: An experimental study. Unpublished Ph.D. Dissertation, Texas A & M University, College Station, Texas.
- Sibson, R. H. 1986. Brecciation process in fault zones: Inferences from earthquake rupturing. *Pure & Appl. Geophys.* **124**, 159–175.
- Srivastava, D. & Engelder, T. 1990. Crack-propagation sequence and pore-fluid conditions during fault-bend folding in the Appalachian Valley and Ridge. *Bull. geol. Soc. Am.* **102**, 116–128.
- Swanson, M. T. 1988. Pseudotachylite-bearing strike-slip duplex structures in the Fort Foster Brittle Zone, S. Maine. *J. Struct. Geol.* **10**, 813–828.
- Swanson, M. T. 1990. Extensional duplexing in the York Cliffs strike-slip fault system, southern coastal Maine. *J. Struct. Geol.* **12**, 499–512.
- Tchalenko, J. S. 1968. The evolution of kink-bands and the develop-

- ment of compression textures in sheared clays. *Tectonophysics* **6**, 159–174.
- Tchalenko, J. S. 1970. Similarities between shear zones of different magnitudes. *Bull. geol. Soc. Am.* **81**, 1625–1640.
- Tchalenko, J. S. & Ambraseys, N. N. 1970. Structural analysis of the Dasht-e Bayaz (Iran) earthquake fractures. *Bull. geol. Soc. Am.* **81**, 4–60.
- Vialon, P. 1979. Les déformations continues-discontinues des roches anisotropes. *Ecol. geol. Helv.* **72**, 53–549
- Wojtal, S. & Mitra, G. 1986. Strain hardening and strain softening in fault zones from foreland thrusts. *Bull. geol. Soc. Am.* **97**, 674–687.